NO$_x$ Removal Catalysis

P. Forzatti, I. Nova, and L. Castoldi

Centro NEMAS – Nano Engineered MAterials and Surfaces
Dipartimento di Chimica, Materiali e Ingegneria Chimica "Giulio Natta"
Politecnico di Milano; Piazza Leonardo da Vinci, 32 – 20133 Milano, Italy

This paper surveys the most important catalytic emission control technologies being employed or near commercialization for the removal of nitrogen oxides (NO$_x$) from the exhausts of mobile sources under lean conditions. Urea/Ammonia-SCR systems and NO$_x$ Storage/Reduction (NSR) catalysts will be addressed, with particular attention to the specific demands related to the mobile applications.

In the first part of the paper the transient kinetics of standard de-NO$_x$ SCR reaction over commercial V-W/Ti SCR catalysts and the dynamic model of the honeycomb reactor will be addressed. Then the validation of the dynamic model with integral reactor measurements and full-scale transients in vehicles will be illustrated.

The second part presents a complete and quantitative understanding of the NO$_x$ storage chemistry of a Pt-Ba/Al$_2$O$_3$ "Lean NO$_x$ Trap" catalyst.

Keywords:
Catalysis, environment, deNO*x*, Urea SCR, NO$_x$ Storage/Reduction (NSR)

Introduction

Lean-burn engines are of growing interest for vehicles since they ensure lower CO$_2$ emissions and improve fuel economy if compared to traditional stoichiometric engines. The **T**hree **W**ay **C**atalyst (TWC) technology, that is worldwide installed in vehicles, realized through the years a significant reduction of CO, NO$_x$, and HC emissions. However, this technology has been optimized for use in exhaust that fluctuates around the oxygen free conditions (i.e. the stoichiometric Air/Fuel ratio) and to date has not resulted in acceptable emission reductions when used in lean burn after-treatment applications. On the other hand upcoming regulations for diesel engines also require significant reductions in NO$_x$ emissions, in the order of 50–60 % in Europe and Japan, and 80–90 % in the US.

Accordingly, new technologies are needed to reduce NO$_x$ to N$_2$ in the oxygen-rich environment without unacceptable fuel efficiency losses. The technologies presently under development are based on two different approaches. The first approach relies on the continuous selective catalytic reduction of NO$_x$ (SCR) and uses a reducing agent that reacts selectively with NO$_x$ rather than with oxygen: this group includes urea- or ammonia-SCR and hydrocarbon SCR. The second approach realizes the removal of NO$_x$ by storing nitrogen oxides under lean conditions and then reducing the stored NO$_x$ to N$_2$ under short, rich excursions: this technology is referred to as NO$_x$ Storage/Reduction (NSR) or Lean NO$_x$ Trap (LNT).

Ammonia/urea-SCR is a mature technology. It is now used worldwide under steady state conditions for the control of NO$_x$ emissions from thermal power plant, cogeneration units, incinerators, and stationary diesel engines.[1] However the large knowledge gained during last decades is not sufficient for the development for mobile applications: indeed, as opposite to the stationary applications, when used in vehicles the catalyst is operated under fast transient conditions so, that a transient kinetics of the de-NO$_x$ reaction and a dynamic model of the catalytic reactor are required. Besides, the system must be operated in a large temperature window, in particular down to low temperatures; this is not typical in standard stationary applications.

Although it has been already commercialised in Japan, NSR is considered a less mature technology, due to a strong sensitivity to fuel S level, which limits the application in Countries where gasoline with low-sulphur content are employed.[2]

In the following we will present and discuss primarily the results collected in our lab at Politecnico di Milano on these two options for NO$_x$ removal in vehicles.

At first after a brief introduction on the fundamentals of ammonia SCR, the transient kinetics of standard de-NO$_x$ reaction over commercial V-W/Ti SCR catalysts and the dynamic model of the honeycomb reactor will be addressed. Then the validation of the dynamic model with integral reactor mea-

surements and full-scale transients in vehicles will be illustrated.

In the second part of this review the chemistry involved in the storage of NO$_x$ over reference NSR catalysts will be presented and discussed and the open issues outlined.

Ammonia/Urea SCR

Ammonia-SCR fundamentals

The SCR process is based on the reduction of NO$_x$ with ammonia into water and nitrogen according to the following main reaction:

$$4 \text{ NO} + 4 \text{ NH}_3 + \text{O}_2 \rightarrow 4 \text{ N}_2 + 6 \text{ H}_2\text{O} \quad (1)$$
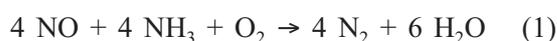
In fact NO accounts for 90–95 % of NO$_x$ in the exhausts.

In the case of sulphur containing fuels (e.g. coal), SO$_2$ is produced during combustion in the boiler along with minor fractions of SO$_3$ (about 1 % of total SO$_x$): SO$_2$ can further be oxidized to SO$_3$ over the catalyst:

$$\text{SO}_2 + 1/2 \text{ O}_2 \rightarrow \text{SO}_3 \quad (2)$$

This reaction is highly undesired because SO$_3$ reacts with water present in the flue gas and with ammonia to form ammonium sulphates. Ammonium sulphates deposit and accumulate onto the catalyst if the temperature is not high enough, leading to catalyst deactivation that can be reversed upon heating.

Commercial SCR catalysts are made of homogeneous mixtures of titania, tungsta and vanadia. Titania in the anatase form is used as high surface and sulphur resistant carrier to support the active components. Tungsta is employed in large amounts ($w = 10$ %) to increase the surface acidity and the thermal stability of the catalyst. Vanadia is responsible for the activity in the reduction of NO$_x$, but it is also very active in the oxidation of SO$_2$. Accordingly its content is kept low, usually below $w = 1–2$ %.

The SCR catalysts are used in the form of honeycomb monoliths or plates to guarantee low pressure drops in view of the large frontal area with parallel channels, high external surface area per unit volume of catalyst, high attrition resistance, and low tendency to fly ash plugging. The SCR monoliths and plates are assembled into standard modules and inserted into the reactor to form catalyst layers.

An important requirement of SCR catalysts, especially for stationary applications and power stations, is to combine high activity in the de-NO$_x$ reaction and very low (almost negligible) activity in the oxidation of SO$_2$ to SO$_3$.

As shown in Figure 1 the intrinsic first order rate constant of NO$_x$ reduction increases linearly with the vanadium content, whereas the intrinsic first order rate constant for the oxidation of SO$_2$ increases more than linearly with the vanadia content.[3] This is consistent with the identification of the active sites for NO$_x$ reduction with isolated V sites as opposite to the active sites for SO$_2$ oxidation that are likely associated with dymeric (or polymeric) sulphated vanadyls, in line with the consolidated picture of the active sites in commercial sulphuric acid catalysts. Accordingly, high dispersion of surface V-oxides must be realized during the impregnation of the tungsta-titania powders with the solution of the vanadium salt, as indeed attained in commercial catalysts, and the vanadia content must be low in any case.
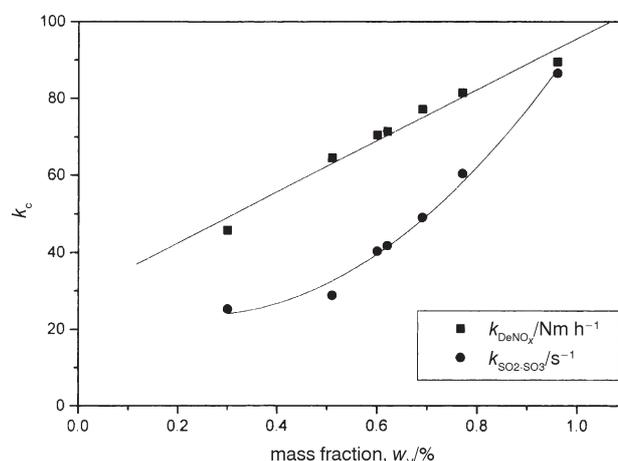
F i g . 1 – *Dependence of the intrinsic kinetic constants of de-NO$_x$ and SO$_2$ oxidation reactions on the catalyst vanadium content at T = 350 °C*

Besides, the reduction of NO$_x$ is a very fast reaction, and is controlled by external and internal diffusion. On the opposite, the oxidation of SO$_2$ is very slow and is controlled by the chemical kinetics. Accordingly the SCR activity is increased by increasing the catalyst external surface area (i.e. the cell density) to favour inter-phase mass transfer, while the activity in oxidation of SO$_2$ is reduced by decreasing the volume of the catalyst (i.e. the wall thickness); this does not affect negatively the activity in NO$_x$ removal because significant ammonia concentrations are confined only near the external geometric surface of the catalyst. Besides a good balance between macro-pores, which guarantee fast diffusion of reagents, and micro-pores, which ensure high activity by providing high catalyst specific surface area, can lead to optimal catalyst performances, in the limit, however, of the required mechanical specifications.[4]

Mechanism and steady state kinetics of the ammonia-SCR reaction

Different proposals have been advanced in the literature for the mechanism of the SCR reaction over vanadia-based catalysts.

One of the first reaction scheme was proposed for the SCR reaction by *Takagi* et al.[5] Their proposal is based on the reaction between co-adsorbed NH$_4^+$ (produced by ammonia adsorption over a V Brønsted acid site) and NO$_2$ (coming from oxidation of NO) via a Langmuir-Hinshelwood mechanism to form nitrogen and water.

Inomata et al.[6] proposed that ammonia is first adsorbed at a Brønsted V site adjacent to a vanadyl and then it reacts with gas-phase NO according to an Eley-Rideal mechanism to form H$_2$O and reduced V species [V(4+)–OH]. The reduced V species is reoxidized by gaseous oxygen.

Based primarily on FT-IR studies, *Busca* et al.[7] suggested that ammonia is adsorbed over Lewis acid site and is activated to form an amide species. The amide species then react with gas-phase NO via a radical coupling to give a nitrosamide intermediate that is known to decompose easily and quantitatively to nitrogen and water. The catalytic cycle is closed by re-oxidation of the reduced catalyst by gaseous oxygen.

Topsøe et al.[8,9] proposed that ammonia is adsorbed at a V Brønsted acid site and is activated by a near-by vanadyl group that is then reduced. NO reacts from the gas-phase with the activated ammonia species leading to the formation of an intermediate, which finally decomposes to nitrogen and water. The catalytic cycle is closed by the re-oxidation of the catalyst by means of gas-phase oxygen.

It is worth noting that, both, mechanisms proposed by Inomata et al. and by Topsøe et al. require the participation of dymeric or polymeric vanadyl species. As an opposite, the mechanism proposed by Busca et al. requires the participation of isolated vanadyls, and this is consistent with the linear dependence of the rate constant of NO$_x$ reduction on the vanadia loading shown in Figure 1. Whatever is the reaction mechanism a key step of the mechanism is represented by the formation of a reaction intermediate that decomposes selectively and quantitatively to nitrogen and water.

Considering that the Eley-Rideal mechanisms discussed above imply the reaction between adsorbed NH$_3$ and gas-phase NO ($r_{NO} = k_c c_{NO} \theta_{NH_3}$) and besides that the reaction is virtually independent of the oxygen partial pressure and is slightly depressed by water up to $\varphi = 5$–10 %, due to competition for adsorption onto the active sites with ammonia, the following kinetic expression has been eventually derived in the literature:[1]

$$r_{NO} = \frac{k_c K_W \, p_{NH_3} \, p_{NO}}{(1 + K_{NH_3} \, p_{NH_3} + K_{H_2O} \, p_{H_2O})} \quad (1)$$

This equation is appropriate in the case of typical stationary SCR applications where a sub-stoichiometric NH$_3$/NO feed ratio is employed to minimize the slip of unconverted ammonia. For high water concentrations (above $\varphi = 5$ % vol.) the dependence of water can be neglected and the following simplified rate equation can be adopted for practical purposes:

$$r_{NO} = \frac{k_c K_{NH_3} \, p_{NH_3} \, p_{NO}}{1 + K_{NH_3} \, p_{NH_3}} \quad (2)$$

which for $K_{NH_3} p_{NH_3} > 1$ (i.e. $r_{NH_3/NO_x} \geq 1$, when full coverage of the surface by NH$_3$ is attained) reduces to (eq. 3):

$$r_{NO} = k_c p_{NO} \quad (3)$$

Equations (2) and (3) have been successfully used by many authors for steady state modelling of the SCR monolith reactor operating with $r_{NH_3/NO_x} < 1$ and > 1 respectively.[10,11,12]

Steady state modelling of the SCR reactor

The customary approach to the design and analysis of monolith SCR reactor, adopted in the technical literature, is based on simple isothermal pseudo-homogeneous single channel lD model that accounts only for the axial concentration gradients inside the channels, whereas the effects of inter-phase and intra-phase mass transfer limitations are lumped into the overall effective pseudo-first order rate constant k$_{NOx}$:

$$k_{NO_x} = - V \ln (1 - \chi_{NO_x}) \quad (4)$$

In eq. (4) V is the superficial velocity, i.e. the ratio of the volumetric flow rate to the overall geometric surface area of the monolith catalyst, χ_{NO_x} represents the fractional conversion of NO$_x$, and k_{NO_x} is given by

$$1/k_{NO_x} = 1/k_c + 1/k_g \quad (5)$$

In fact, the reaction operates under combined intra-particle and external diffusion control: k_c is the effective rate constant of the surface chemical reaction incorporating the influence of mass transfer in catalyst pores ($k_c = \eta \, k_{SCR}$ with η = catalyst internal efficiency and k_{SCR} = intrinsic kinetic coefficient of the SCR reaction) and k_g represents the inter-phase gas-solid mass transfer coefficient.

It has been demonstrated that the gas-solid mass transfer coefficient can be estimated by analogy with the Graetz-Nusselt problem governing heat transfer to a fluid in a duct with constant wall temperature ($Sh = Nu_T$), according to the expression $Sh = Nu_{\infty T} + 6.874\ (1{,}000\ z^*) - 0.488\ \exp\ (-57.2\ z^*)$,[13] which accounts for the entrance effects.

Figure 2 compares the axial concentration profiles of the 1D model with those of the rigorous multidimensional model of the SCR monolith reactor in the case of square channels, that are most common in industrial applications, and of Eley-Rideal kinetics, which must be introduced in place of the first order kinetics (Eq.3) to comply with industrial conditions for steady state applications (substoichiometric $r_{NH_3/NO}$ feed ratio, i.e. $r_{NH_3/NO} < 1$). It is apparent that the 1D model is equivalent to the rigorous multidimensional model.[13]
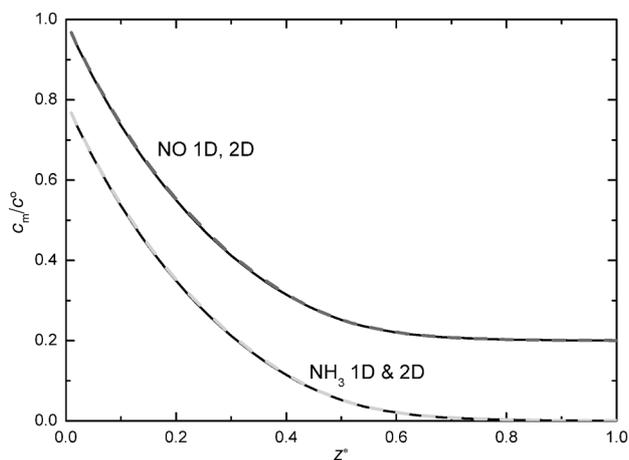
F i g . 2 – *Comparison between calculated axial concentration profiles of NO and NH$_3$ obtained by the lD model and by a rigorous multidimensional model of the SCR monolith reactor*

The study of the intra-phase mass transfer in SCR reactors has been addressed by combining the equations for the external field with the differential equations for diffusion and reaction of NO and NH$_3$ in the intra-porous region and adopting the Wakao-Smith random pore model to describe the diffusion of NO and NH$_3$ inside the pores.[13,14] The solution of the model equations confirmed that under typical industrial conditions the internal catalyst effectiveness factor is low, due to the presence of steep reactant concentration gradients near the external catalyst surface.[12]

Predictions of the model compared successfully with laboratory data collected over honeycomb catalysts of various lengths and under a variety of experimental conditions. For these validations the model did not include any predictive pa-

rameter: the effective diffusivities of NO and NH$_3$ were estimated from the pore size distribution measurements and the intrinsic rate parameters were obtained from independent kinetic data collected over the same catalyst ground to very fine particles.[12]

Dynamic modelling of ammonia-SCR

The study of the dynamics of the ammonia-SCR reaction was addressed by investigating first the adsorption-desorption kinetics of NH$_3$ and NO and then the surface reaction.[15]

In the case of NH$_3$ a typical result obtained upon a rectangular step feed in flowing He+O$_2$ over a ternary home-made V$_2$O$_5$–WO$_3$/TiO$_2$ catalyst at 280 °C is presented in the Figure 3. The results of the TPD experiment obtained upon heating the catalyst from RT up to 500 °C at the end of the ammonia adsorption are also presented. Upon the NH$_3$ step addition (at $t = 0$ s), the ammonia reactor outlet concentration slowly increased with time, approaching the ammonia inlet molar fraction ($\chi = 700 \cdot 10^{-6}$) only after ≈ 500 s. This clearly indicates that ammonia is involved in adsorption-desorption processes at the catalyst surface. Along similar lines, upon the ammonia shut-off ($t = 1000$ s) the reactor outlet NH$_3$ concentration slowly decreases with time due to the desorption of previously adsorbed ammonia. Complete desorption of NH$_3$ is not yet achieved after 2200 s, but could only be achieved by heating the catalyst at high temperature. The results confirm that the adsorption of ammonia is very fast and that ammonia is strongly adsorbed onto the catalyst surface.

The NH$_3$ dynamic adsorption-desorption experiments were also performed at different temperatures, in the range 220–400 °C. On increasing the
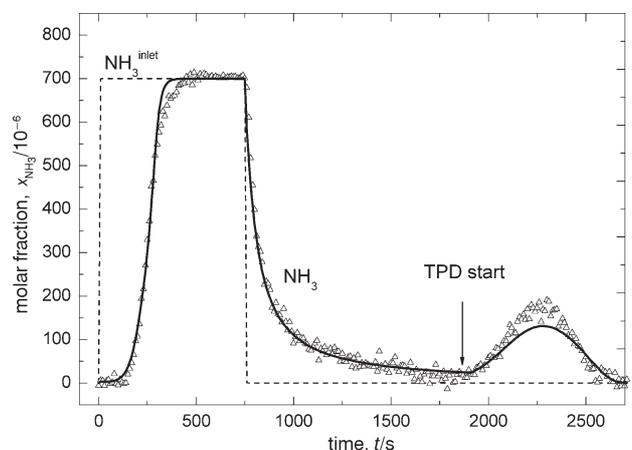
F i g . 3 – *Adsorption – desorption of NH$_3$ at T = 280 °C on a model V$_2$O$_5$-WO$_3$/TiO$_2$ catalyst. Dashed lines: ideal inlet NH$_3$ concentration; symbols (triangles): outlet NH$_3$ concentration; solid line: model fit (Temkin-type coverage dependence)*

catalyst temperature, the variations in the ammonia outlet concentration during the adsorption step are faster and the amount of ammonia adsorbed on the catalyst surface is reduced, in line with the increased rates of the adsorption-desorption processes and with the exothermicity of NH$_3$ adsorption.

Similar experiments were performed for NO,[15] which indicated that it does not appreciably adsorb onto the catalyst surface, in line with previous literature indications.

The dynamics of the SCR reaction was investigated upon performing step changes of the ammonia reactor inlet concentration in flowing He + NO + O$_2$, and step changes of the NO reactor inlet concentration in flowing He + NH$_3$ + O$_2$.

Figure 4 shows typical results obtained over model V$_2$O$_5$-WO$_3$/TiO$_2$ sample upon performing step changes of the NH$_3$ inlet concentration (dashed line) at 220 °C in flowing He + NO ($\chi = 700 \cdot 10^{-6}$) + O$_2$ ($\varphi = 1 \cdot 10^{-2}$). The figure reports the evolution with time of NH$_3$, N$_2$, and NO molar fractions.
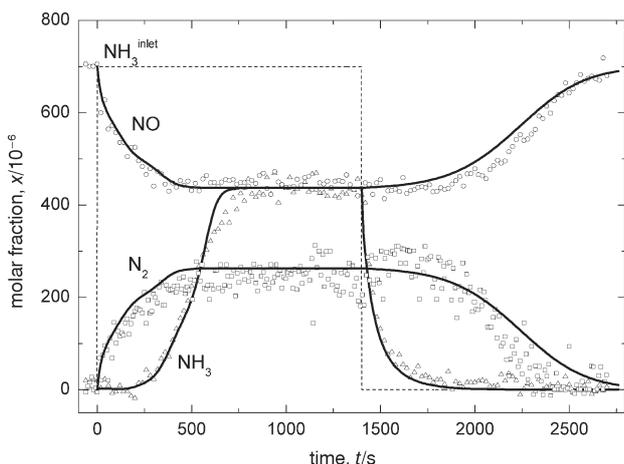
F i g . 4 – *Step feed and shut off of NH$_3$ in He + O$_2$ ($\rho = 1$ %) + NO (700 · 10^{-6}) over a WO$_3$-V$_2$O$_5$/TiO$_2$ model catalyst ($w_{V_2O_5} = 1.47$; $w_{WO_3} = 9$ %) at 220 °C. Dashed lines: ideal inlet NH$_3$ concentration; symbols: outlet concentrations (triangles: ammonia, squares: N$_2$, circles: NO); solid lines: model fits (Temkin-type coverage dependence and "modified kinetics" Eq.(13)).*

Upon the NH$_3$ step feed the outlet reactor concentration decreases and that of N$_2$ shows a symmetric change indicating the occurrence of a genuine SCR process. The ammonia fraction profile exhibits a dead time and then increases with time to the final steady state value that is consistent with the occurrence of the SCR reaction. Upon the shut-off of ammonia at the reactor inlet the ammonia fraction at the reactor outlet rapidly dropped to zero, but the NO and nitrogen fraction signals were not affected for several minutes. Then the NO fraction signal began to increase up to the inlet fraction

value; again the N$_2$ fraction trace is symmetrical to that of NO. These data suggest that the rate of the SCR reaction is unaffected by changes in the ammonia surface coverage at high ammonia coverage. Similar results were obtained by performing the NH$_3$ step-feed experiments at higher temperatures (280 and 350 °C): the results were found in line with, both, the exothermicity of the NH$_3$ adsorption and with the increased rate of the surface reaction, which result in lower ammonia surface coverage.

The adsorption-desorption and reaction kinetic data were analyzed by means of a dynamic 1D isothermal heterogeneous PFR model of the laboratory microreactor and fitted by nonlinear regression to provide the estimates of the relevant kinetic parameters.[15] The influence of both intra-particle and external mass transfer limitations were estimated as negligible, on the basis of theoretical diagnostic criteria.[16] The complete unsteady state model for adsorption-desorption and surface reactions was based on the following equations, with symbols defined in the Notation section:

NH$_3$ mass balance on the catalyst surface:

$$\frac{\partial \theta_{NH_3}}{\partial t} = r_a - r_d - r_{NO} - r_{OX} \tag{6}$$

NH$_3$, NO and N$_2$ mass balances on the gas stream:

$$\frac{\partial c_{NH_3}}{\partial t} = -v \frac{\partial c_{NH_3}}{\partial z} + C_{NH_3} \cdot (r_a - r_d - r_{NO} - r_{0X}) \tag{7}$$

$$\frac{\partial c_{NO}}{\partial t} = -v \frac{\partial c_{NO}}{\partial z} + \Omega_{NH_3} \cdot r_{NO} \tag{8}$$

$$\frac{\partial c_{N_2}}{\partial t} = -v \frac{\partial c_{N_2}}{\partial z} - \Omega_{NH_3} \cdot (r_{NO} + 0.5 \cdot r_{0X}) \tag{9}$$

rate expressions:

$$r_a = k_a^0 \cdot e^{-E_a/RT} \cdot c_{NH_3} \cdot (1 - \theta_{NH_3}) \tag{10}$$

$$r_d = k_d^0 \cdot e^{-E_d/RT} \cdot \theta_{NH_3} \tag{11}$$

$$r_{ax} = k_{ax}^0 \cdot e^{-E_{ax}/RT} \cdot \theta_{NH_3} \tag{12}$$

$$r_d = k_d^0 \cdot e^{-E_d/RT} \cdot c_{N0} \cdot \theta_{NH_3}^* \cdot (1 - e^{\theta_{NH_3}/\theta_{NH_3}^*}) \tag{13}$$

Thus, in addition to adsorption and desorption of ammonia (r_a and r_d, respectively) and to its surface reaction with NO to give nitrogen and water (r_{NO}), also ammonia oxidation (r_{ox}) was introduced in order to account for the direct oxidation of ammonia occurring at high temperatures. C_{NH_3} in the equations represents the catalyst NH$_3$ adsorption capacity (mol m^{-3}).

Eq. (6)-(9) were solved by standard numerical procedures[17,18] and the data fit was performed on the experimental results, as shown in the figures 4 and 5 for selected NH$_3$ adsorption-desorption experiments, and runs with changes in the NH$_3$ reactor inlet concentration in flowing NO + O$_2$. The data fit is reported as solid lines in the same figures: it appears that the goodness of fit is satisfactory. The activation energy for NH$_3$ adsorption was found to be close to zero, and accordingly a non-activated ammonia adsorption process was considered in the model (E$_a$ ≈ 0). Besides, a Temkin-type ($E_d = E_d^0 \cdot (1 - \gamma \cdot \theta_{NH_3})$) coverage dependence of the desorption energy had to be used to describe the adsorption desorption data; indeed a simple Langmuir approach (that considers a constant value of the desorption activation energy) was not appropriate. This is consistent with the presence of distinct types of acid sites (Lewis and/or Brønsted) characterized by different acid strengths at the catalyst surface.[19]
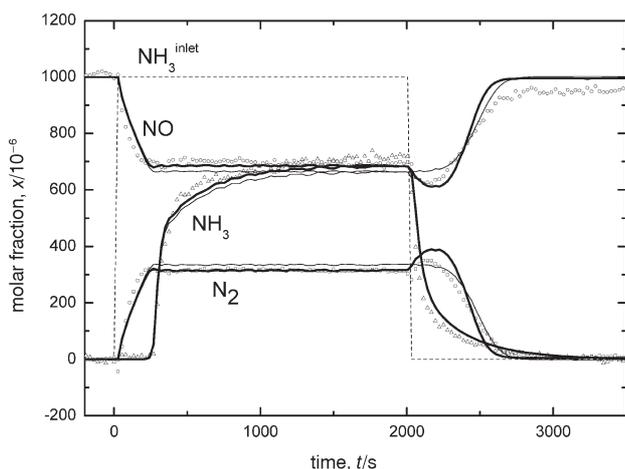
F i g . 5 – *Step feed and shut off of NH$_3$ in He + O$_2$ (ρ = 2 %) + H$_2$O (ρ = 1 %) + NO (1.0 · 10^{-3}) over a WO$_3$-V$_2$O$_5$/TiO$_2$ commercial catalyst at 175 °C. Dashed lines: ideal inlet NH$_3$ concentration; symbols: outlet concentrations (triangles: ammonia, squares: NO, circles: N$_2$); solid thin lines: kinetic fit by "modified kinetics" – Eq.(13); solid thick lines: kinetic fit by modified Redox rate expression – Eq.(14).*

To describe quantitatively the reactivity data a "modified θ_{NH_3} kinetics" Eley-Rideal (eq.(13)) had to be adopted:[15] this empiric expression assumes that r_{NO} is essentially independent of the ammonia surface coverage above a critical NH$_3$ coverage ($\theta_{NH_3}^*$). This has been explained assuming that a "reservoir" of NH$_3$ species, adsorbed on poorly reactive and most abundant W and Ti sites, is present and available for the reaction upon ammonia desorption followed by re-adsorption at the active V sites. Indeed, the analysis of the rate parameters estimated by fitting the dynamic data indicated that the rate of ammonia adsorption is comparable to the

rate of surface reaction, whereas ammonia desorption is much slower. Accordingly, the assumption of equilibrated adsorption, which is usually assumed in the kinetic studies available in the literature, may be incorrect.

More recently specific attention was paid to transient experiments in the low-T region: accordingly dedicated dynamic experiments have been performed on a commercial V$_2$O$_5$-WO$_3$/TiO$_2$ catalyst.[20]

Figure 5 shows data recorded at 175 °C feeding NH$_3$ step pulses (0 → 1000 → 0 ppmv) in flowing He + NO (1000 ppmv) + O$_2$ (2 % v/v) + H$_2$O (1 % v/v): the measured temporal evolutions of NH$_3$ (circles), NO (squares), and N$_2$ (triangles) outlet fractions are plotted. It is worth noticing that at t = 1500 s, when ammonia is removed from the feed stream, the NO concentration trace decreases, goes through a minimum and then begins to increase, recovering the inlet value when the reaction is depleted. The symmetrical evolution of N$_2$ confirmed the occurrence of the SCR reaction. Similar effects, always observed in transient experiments performed under equivalent conditions and T < 250 °C and reported in the past over different commercial SCR catalysts for stationary applications,[21,22] were attributed to an inhibiting effect of excess NH$_3$, possibly caused by a competition between NO and ammonia in adsorbing onto the catalyst. Such inhibition effects are of limited interest for stationary applications of the SCR technology, but may play a considerable role in mobile applications, since they become more significant at low temperatures, and also affect the dynamic response of the SCR systems.

The peculiar dynamic effect attributed to the inhibition effect of ammonia, has been recently accounted for by a dual-site modified Redox rate law (MR)[20]

$$r_{NO} = \frac{k_{NO}'^{0'} \exp\left(-\dfrac{E_{NO}}{RT}\right) c_{NO} \theta_{NH_3}}{1 + K_{NH_3}' \dfrac{\theta_{NH_3}}{1 - \theta_{NH_3}}} \left(\frac{p_{O_2}}{0.02}\right)^{\beta} \quad (14)$$

that assumes competition between ammonia and NO in adsorbing onto the catalyst. This model provides a much better description of the observed dynamics than the previously employed Eley-Rideal kinetics.

In Figure 5 the fit results obtained by using either the MR rate expression, Eq. (14), (solid thick lines) or the "modified θ_{NH_3} kinetics" ER kinetics, Eq. (13), (solid thin lines) are compared: it clearly appears that the redox kinetics account better for

the transient maxima-minima features of the experimental trace during the NH$_3$ shutdown phase.

The MR kinetic model has been then validated on a predictive basis by comparing its simulations with experimental data from microreactor runs consisting of high frequency NH$_3$ feed pulses in a stream of 1000 ppmv of NO, 2 % v/v O$_2$ and 1 % v/v H$_2$O.[20] The experimental signals were in line with the above-mentioned ammonia inhibition effect, exhibiting a characteristic transient behaviour, characterized by a greatest NO conversion after the NH$_3$ shut down.

The experiments were simulated using both the MR, Eq. (14), and the "modified θ_{NH3} kinetics" ER, Eq. (13), rate expressions. The results confirmed that changing the DeNO$_x$ rate equation from the ER-based to the new MR kinetic model improved significantly the description of fast SCR transients similar to those associated with the operation of SCR after treatment devices for vehicles.

A single channel dynamic model of the monolith reactor has also been developed, which accounts for internal and external diffusion along the lines already outlined in the case of the stationary model. Enthalpy balances in this case are included to cope with fast temperature excursion associated with load changes of the engine in the vehicles.[20]

The model consists of unsteady mass and enthalpy balances in the gas phase and in the solid phase with the appropriate initial and boundary conditions, as shown in the following with symbols defined in the Notation section:

gas phase:

$$\frac{\partial c_j}{\partial t} = -\frac{v}{L}\frac{\partial c_j}{\partial z} - \frac{4}{d_h}k_{m1,j}(c_j - c_j^w)$$
$$j = NH_3, NO \tag{15}$$

$$\frac{\partial T_g}{\partial t} = -\frac{v}{L}\frac{\partial T_g}{\partial z} - \frac{4}{d_h}(T_g - T_s)/(\rho_g c_p) \tag{16}$$

solid phase:

$$0 = k_{m1,j}(c_j - c_j^w) + r_{eff,j} \quad j = NH_3, NO \tag{17}$$

$$\frac{\partial T_s}{\partial t} = \frac{h(T_g - T_s) - \sum_{j=1}^{NCG}\Delta H_j r_{eff,j}}{\rho_s c_{p,s}\delta_W(1 + \delta_W/d_h)} \tag{18}$$

diffusion-reaction of the reactants in the catalytic monolith walls

$$0 = D_{eff,j}\frac{\partial^2 c_j^*}{\partial x^2} + S_W^2 R_j \quad j = NH_3, NO \tag{19}$$

$$r_{eff,j} = \frac{D_{eff,j}}{\delta_W}\left.\frac{\partial c_j^*}{\partial x}\right|_W \quad j = NH_3, NO \tag{20}$$

accumulation/depletion of NH$_3$ adsorbed onto the catalyst surface

$$c_{NH_3}\frac{\partial \vartheta_{NH_3}}{\partial t} = r_{NH_3} \tag{21}$$

In addition to rate parameters and reaction conditions, the model requires the physico-chemical, geometrical, and morphological (porosity, pore size distribution) characteristics of the monolith catalyst as input data. Effective diffusivities, $D_{eff,j}$, are then evaluated from the morphological data according to a modified Wakao-Smith random pore model.

The model has been validated at DaimlerChrysler against a large number of transient experiments with step pulses of NH$_3$ in a continuous flow of NO over monolith catalyst samples (typically with 10 cm^3 volume and 200 cpsi cell density).[23] Validation maps were generated using the steady state measured engine operating points and the deviation between simulated NO$_x$ conversion and experimental data was typically below 4 %.

The reactor model was also validated by performing engine test bench experiments under real conditions in the *T* range 150–450 °C (using extruded monoliths with 300 cpsi, a wall thickness of 0.32 mm and a monolith diameter of 11 mm) with ETC (European Transient Cycle) and ESC (European Stationary Cycles) measurement.

Figure 6 shows the model simulations (grey lines) and experimental results (solid black lines) for NO$_x$ concentrations downstream of the catalyst along with the inlet NO$_x$ concentration values. The comparison between measurement and simulation for the NO$_x$ reveals that an excellent correlation was obtained for both the cycles. The mean error of the model predictions in the deNO$_x$ efficiency was not higher than 3–4 %.

These results confirm that the model is able to predict accurately the dynamic behaviour of SCR monolith catalysts under fast transient conditions.

Such results were achieved only by using the MR rate (eq. (14)); indeed, the adoption of a classic Eley-Rideal rate law or of a modified θ_{NH3} kinetics Eley-Rideal (eq.(13)), resulted in a significantly less accurate prediction of the NO$_x$ conversion during the fast transient parts of the test cycles.

The ammonia-SCR for Heavy-Duty diesel engine is now commercialized by DaimlerChrysler as an after treatment system able to satisfy, both, the EURO IV and V legislations.
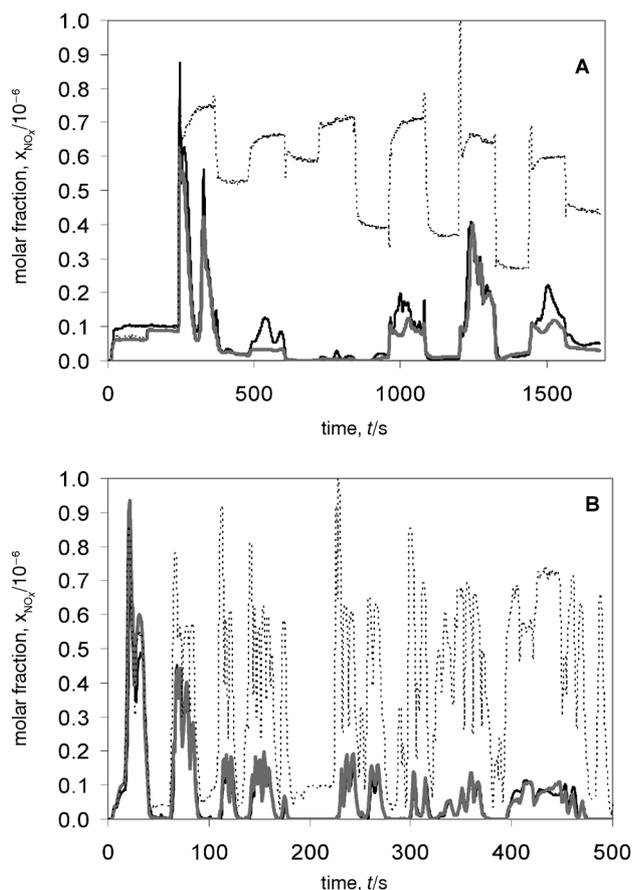
F i g . 6 – *Normalized NO$_x$ concentration at SCR catalyst inlet and outlet of an ESC (A) and an ETC (B) test cycle. Dotted black lines – inlet values, solid black lines – outlet measurement, grey lines – outlet simulation.*

Conclusions

The dynamic study performed on the SCR reaction proved to be a very useful and unique tool, as it helped in clarifying kinetic and mechanistic aspects of the SCR process. These include the following:

i) a "reservoir" of adsorbed NH$_3$ species is present on the catalyst surface and is available for the reaction via desorption and subsequent fast re-adsorption;

ii) a comparison among the estimates of the adsorption, desorption, and reaction rates calculated at different reactor axial position, temperatures and catalysts indicates that the assumption of equilibrated ammonia adsorption under steady-state DeNO$_x$ conditions is incorrect, specifically at high temperatures and over active catalysts;

iii) the rate of the SCR reaction at low temperature is lower in presence of excess ammonia, that is ammonia plays an inhibiting effect on the deNO$_x$ conversion; the use of an adequate kinetics is mandatory to predict fast transient experiments where ammonia concentration changes continuously;

iv) a single dynamic two phase, 1D+1D model of the honeycomb reactor, was found to describe properly fast transient experiments performed on a real Heavy Duty engine test bench facility with an urea-SCR system.

NO$_x$ Storage/Reduction technology

The NO$_x$ Storage/Reduction technology represents an alternative to urea- or ammonia-SCR technology for the removal of NO$_x$ under lean conditions.

In the NSR process, NO$_x$ are stored under lean conditions in the form of nitrites and nitrates and are reduced to nitrogen during a short rich excursion. The NSR catalysts typically consist of a NO$_x$ storage component, such as an alkaline earth metal oxide (e.g. Ba), and of a noble metal (e.g. Pt) that catalyzes the oxidation of NO$_x$, CO, and of hydrocarbons and the reduction of stored NO$_x$ as well.

NO$_x$ storage mechanism

The NO$_x$ storage process has been extensively investigated primarily by dynamic methods and in situ spectroscopy,[24–30] but a detailed understanding of the NO$_x$ storage mechanism and reliable kinetics are still lacking.

An extensive study of NO$_x$ storage over an homemade reference Pt-Ba/Al$_2$O$_3$ system has been performed in our laboratories, and the results are reported in various papers.[31–36] In particular, in order to clarify the adsorption process under realistic operating conditions, the adsorption of NO in presence of oxygen has been recently investigated in our laboratories[37] over a Pt-Ba/γ-Al$_2$O$_3$ sample. The study has also investigated the adsorption of NO$_2$ that many authors recognize as intermediate in the NO$_x$ storage process. To better enlighten the nature and the evolution of the stored NO$_x$ species and the role of the catalyst component in the NO$_x$ storage process, the adsorption of NO and of NO$_2$ in the presence and in the absence of oxygen were carried out in a fixed bed flow microreactor at 350 °C over Pt-Ba/Al$_2$O$_3$ ternary catalysts with different Ba loading, over the corresponding binary Ba/Al$_2$O$_3$ and Pt/Al$_2$O$_3$ samples, and over the bare γ-Al$_2$O$_3$ support.

The γ-alumina support was obtained by calcination at 700 °C of a commercial alumina material; Pt/Al$_2$O$_3$ ($\zeta = 1/100$) and Ba/Al$_2$O$_3$ ($\zeta = 20/10$) catalysts were prepared by incipient wetness impregnation of the alumina support with aqueous solutions of dinitro-diammine platinum or barium acetate. The powders were then dried overnight in air at 80 °C and finally calcined at 500 °C for 5 h. The

Pt-Ba/Al$_2$O$_3$ (ζ = 1/x/100) samples with different barium loading (5–30 %) were prepared by impregnation of calcined Pt/Al$_2$O$_3$ with different solutions of barium acetate.[31,37]

The adsorption of NO$_x$ under lean conditions has been investigated by performing transient experiments where a step change of NO and NO$_2$ was imposed in the presence and absence of oxygen at 350 °C over reference catalysts and analyzing the transient response in the outlet concentrations of reactants and products (Transient Response Method); the stored NO$_x$ species were then removed from the catalyst surface by performing a TPD run up to 600 °C. FT-IR was used as a complementary technique to investigate the nature of the stored NO$_x$ species.

The adsorption of NO$_2$ over the Ba(16)/γ-Al$_2$O$_3$ sample has been investigated at first. In fact, NO$_2$ has been suggested as intermediate in the NO adsorption in the presence of oxygen.[24] As shown in Figure 7A, the storage of NO$_2$ over the Ba(16)/γ-Al$_2$O$_3$ sample is accompanied by the evolution of NO in the gas phase, which is observed

without any dead time; large amounts of NO$_x$ are stored at the end of the pulse, near 9E-04 mol g$_{cat}$$^{-1}$. FTIR spectra (Figure 7B) collected upon contacting the catalyst with NO$_2$ show that only nitrates are formed. The nitrate species adsorbed over Ba/γ-Al$_2$O$_3$ show high thermal stability; as a matter of fact, during the subsequent TPD experiment, NO$_2$ desorption was observed starting from 370 °C with a maximum at 470 °C, while NO and oxygen show peaks at higher temperature (with maxima close to 560 °C).

In agreement with literature[2,27,31] the nitrates are primarily formed through a NO$_2$ disproportionation reaction, following the overall stoichiometry:

$$BaO + 3\ NO_2 \rightarrow Ba(NO_3)_2 + NO \uparrow \qquad (3)$$

that also accounts for the evolution of NO.

It is worth noting, that over the supported Ba sample the Integral Molar Ratio of NO evolved to NO$_2$ consumed (Figure 8), that is equal to 1/3 according to the disproportionation reaction, is initially lower than the stoichiometric value. This indicates that the NO$_2$ uptake at the beginning of the

F i g . 7 – *Results of NO$_2$ adsorption TRM experiments in He at 350 °C and subsequent TPD in terms of NO, NO$_2$, NO$_x$, O$_2$ outlet concentrations and NO$_2$ inlet concentration over A) Ba/γ-Al$_2$O$_3$; C) Pt-Ba/γ-Al$_2$O$_3$ catalysts. Results of NO$_2$ adsorption FT-IR experiments over B) Ba/γ-Al$_2$O$_3$, D) Pt-Ba/γ-Al$_2$O$_3$ catalysts. Spectra are reported after 1 and 10 min of exposure to 5 mbar of NO$_2$ at 350 °C. Each spectrum is reported as difference from the spectrum before NO$_2$ admission.*

pulse does not obey the overall stoichiometry of reaction (3); however, the stoichiometric value is roughly approached at the end of the pulse. This has been explained in the literature[24]. considering that the NO$_2$ disproportionation consists of consecutive elementary steps:

$$NO_2 + BaO \rightarrow BaO\text{-}NO_2 \qquad (4)$$

$$BaO\text{-}NO_2 \rightarrow BaO_2 + NO \qquad (5)$$

$$BaO_2 + 2\ NO_2 \rightarrow Ba(NO_3)_2 \qquad (6)$$
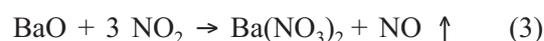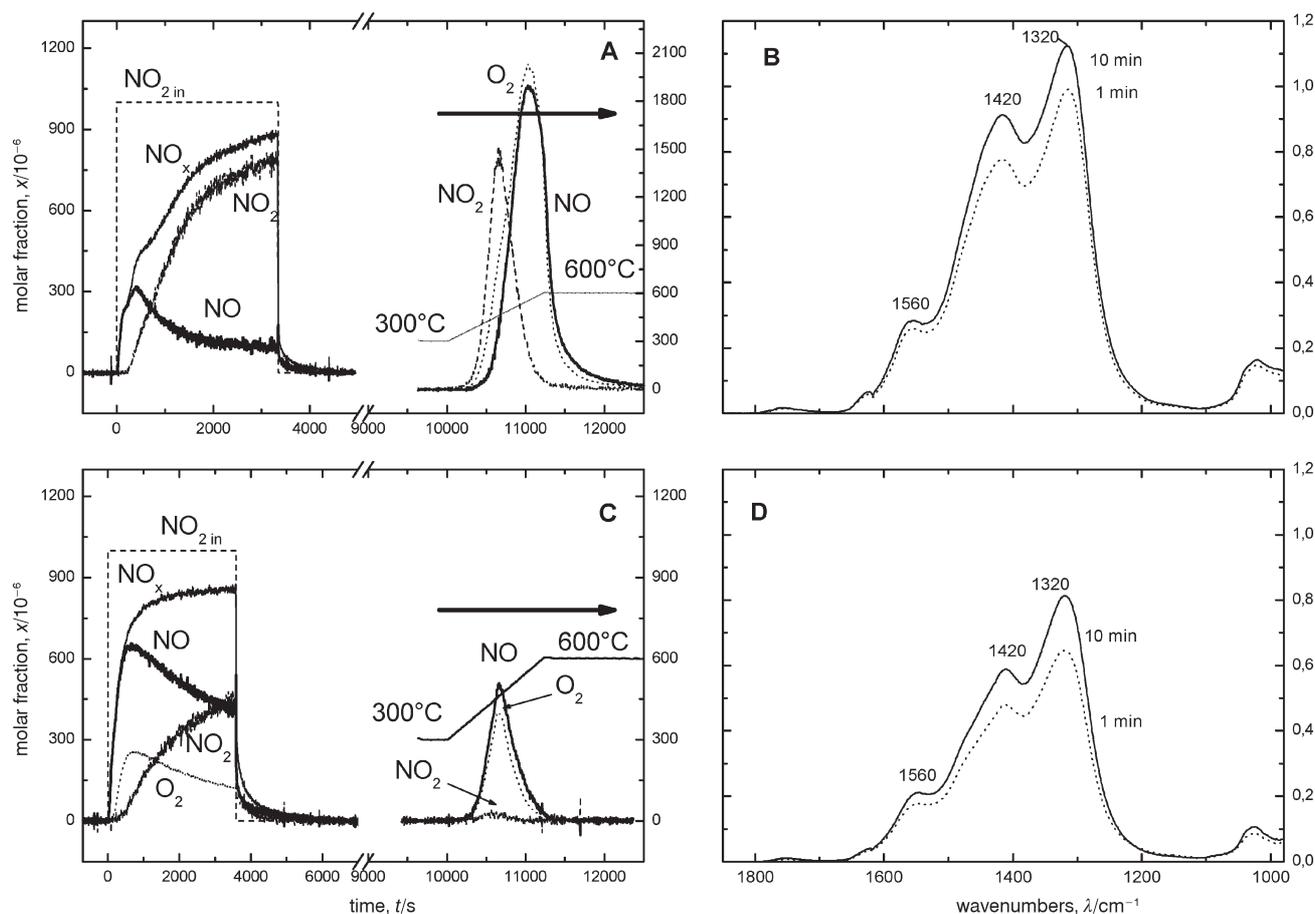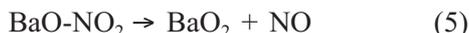
and that the first step is fast as compared to the following ones, which account for the evolution of NO.

NO$_2$ adsorption experiments have been also performed over the Pt-Ba(16)/γ-Al$_2$O$_3$ sample (Figure 7C). The formation of NO is observed, showing a maximum of about 600 ppmv, without any significant dead time. On the other hand, NO$_2$ fraction shows a dead time (280 s) followed by a slow increase. O$_2$ formation has also been observed in this case, pointing out that NO$_2$ is decomposed to NO and oxygen over Pt. FTIR spectra collected over Pt-Ba/γ-Al$_2$O$_3$ catalysts (Figure 7D) pointed out that mainly nitrate species were formed upon NO$_2$ adsorption. The TPD run performed to regenerate the ternary system showed the evolution of NO and oxygen at lower temperatures with respect to Ba/γ-Al$_2$O$_3$ (470 vs. 560 °C), while NO$_2$ evolution was not observed. These features can be ascribed to the presence of Pt, which favors both the decomposition of nitrate species and of NO$_2$.

The results of NO$_2$ adsorption over Pt-Ba(16)/Al$_2$O$_3$ has been rationalized by considering three distinct functionalities: i) at the beginning ($t = 0$–50 s), NO$_2$ adsorption occurs through the mechanism already proposed for Ba/γ-Al$_2$O$_3$, which results in the formation of nitrate species without NO release or considering a fast occurrence of the first step of the disproportionation reaction (reaction (4)) and a slower rate for the subsequent steps responsible for the evolution of NO (reactions (5) and (6)); ii) after 50 s the slower elementary steps of the disproportionation route are proceeding, leading to formation of surface Ba-nitrates with NO evolution; iii) while the NO$_2$ storage on Ba further proceeds, the Pt-catalyzed NO$_2$ decomposition to NO and O$_2$ becomes appreciable, as pointed out by the evolution of O$_2$.

The adsorption of NO/O$_2$ on the Ba(16)/γ-Al$_2$O$_3$ sample has also been investigated (Figure 9A). In this case, the binary sample adsorbs minor amounts of NO, which is immediately observed at the reactor outlet without any dead time. The FTIR spectra recorded at different exposure times are displayed in Figure 9B; ionic nitrites (1220 cm^{-1}) were pro
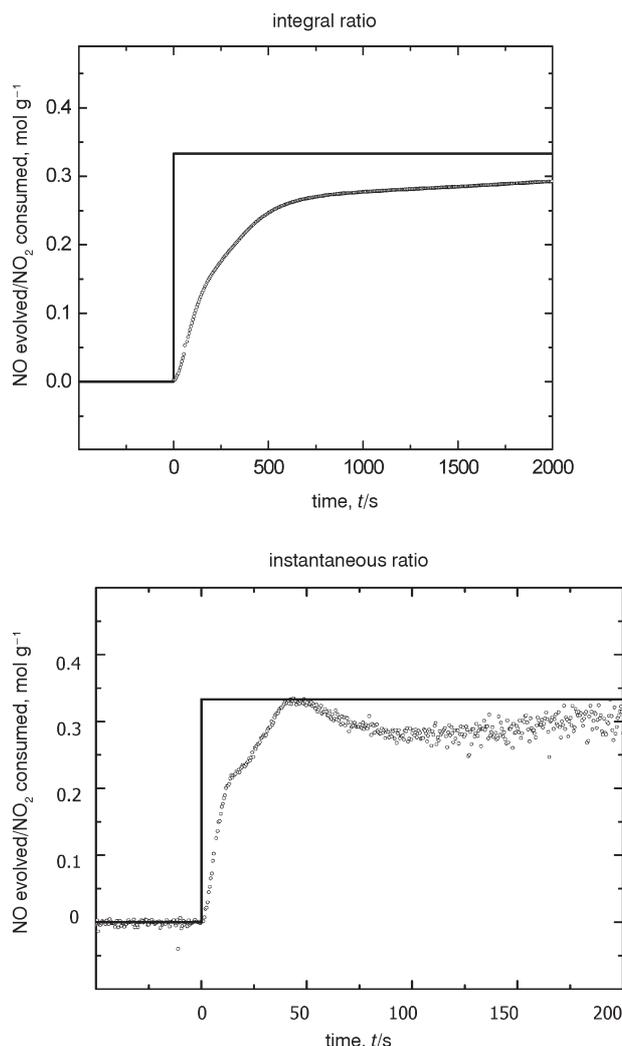
F i g . 8 – *Ratio of NO evolved to the amounts of NO$_2$ stored in He over Ba/γ-Al$_2$O$_3$ catalyst*

gressively formed on increasing the exposure time, along with small amounts of bridging nitrates. At higher exposure times, the band due to nitrite species decreased in intensity and completely disappears after 20 min. In parallel, bands characteristic of ionic nitrate develop, so that at catalyst saturation only nitrates are present in the spectra.

When the storage phase is carried out starting from NO/O$_2$ mixtures over the Pt-Ba(16)/γ-Al$_2$O$_3$ catalyst (Figure 9C) the situation is significantly modified: both, NO and NO$_2$ outlet fraction showed a significant delay, indicative of a complete uptake of NO$_x$ species, and peculiar feature of the ternary catalyst. Also, in this case the system is able to adsorb large amounts of NO$_x$ (4.6E-04 mol g$_{cat}^{-1}$ up to catalyst saturation). Besides NO is readily oxidized to NO$_2$ over Pt. As observed in the case of Ba/alumina catalyst, FT-IR spectra (Figure 9D) showed, that the adsorption of NO initially occurs primarily in the form of nitrites, that are readily transformed
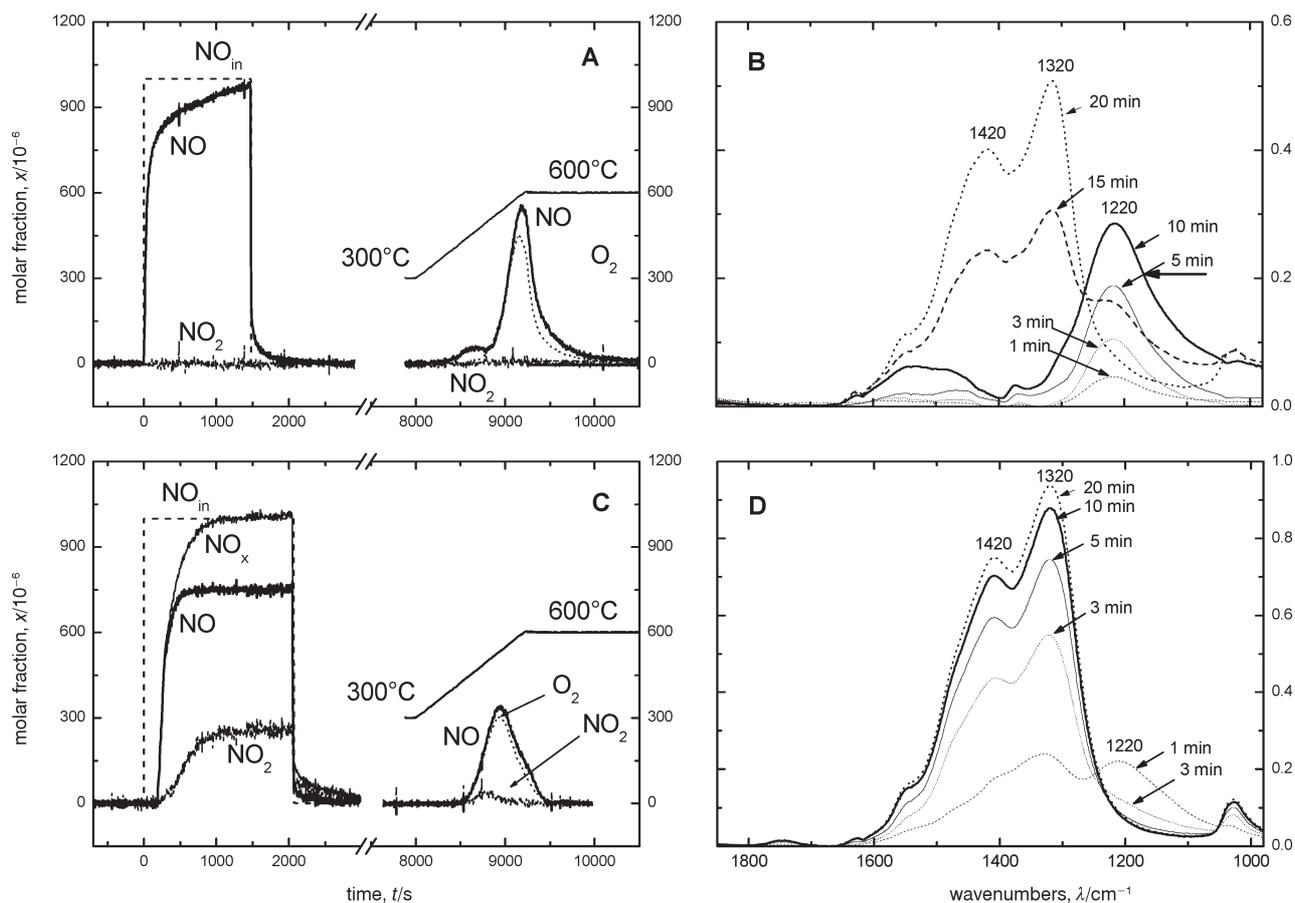
F i g . 9 – *Results of NO adsorption TRM experiments at 350 °C in He+O_2 and subsequent TPD in He in terms of NO, NO_2, NO_x, O_2 outlet fraction and NO inlet fraction over A) Ba/γ-Al_2O_3, C) Pt-Ba/γ-Al_2O_3 catalysts. Results of NO/O_2 adsorption FT-IR experiments over B) Ba/γ-Al_2O_3, D) Pt-Ba/γ-Al_2O_3 catalysts. Spectra are reported after 1, 3, 5, 10, 15 and 20 min of exposure to NO/O_2 mixtures (1:4, p_{NO} = 5 mbar) at 350 °C. Each spectrum is reported as difference from the spectrum before NO/O_2 admission.*

into nitrates over Pt. Notably, the rate of, both, nitrite formation and their oxidation to nitrates are higher on Pt-Ba/γ-Al_2O_3 than on Ba/γ-Al_2O_3, pointing out a catalytic role of Pt. This situation was also confirmed by DRIFT data (Figure 10) collected under *operando* conditions equal to those used in the TRM experiments, showing that during the initial NO_x uptake nitrites are more abundant than nitrates: the nitrite band intensity showed a broad maximum and then decreased with time on stream, while the nitrate bands presented a monotonous increase during the entire storage phase, so that at the end of the experiment (at ca. 700 s) nitrates are the most abundant adsorbed species. Thus, in line with FTIR data, in the adsorption process nitrites are intermediate species which then evolve leading to the formation of nitrates. Notably, the maximum in the nitrite band intensity corresponded roughly to the NO breakthrough observed by TRM experiments and confirmed by the analysis of data collected with the quadrupole mass-spectrometer interfaced with the DRIFT cell.

All the previous data led to the proposal of the following reaction pathways (Figure 11) for the
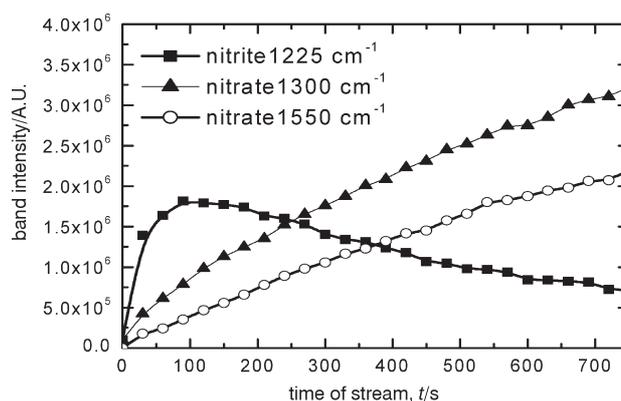
F i g . 1 0 – *Results of NO/O_2 adsorption DRIFT experiment over Pt-Ba/Al_2O_3 plots of band maxims vs. time*

storage of NO_x over Pt-Ba/alumina catalysts. In the presence of oxygen NO is effectively stored through a stepwise oxidation at a Pt site followed by adsorption at a neighboring Ba site to form Ba-nitrites at first and Ba-nitrates later on. The proximity of Pt and Ba sites likely results in the stabilization of nitrites against further oxidation to nitrates. This is referred to as the *nitrite route.*
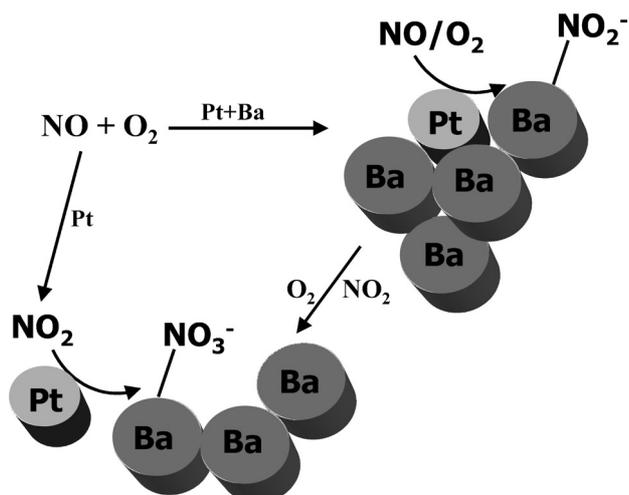
F i g . 1 1 – *Reaction pathway for NO_x adsorption over sup-ported Pt-Ba catalysts*

NO is also oxidised to NO_2 over Pt in the presence of oxygen. NO_2 can be adsorbed onto the Ba sites to form Ba nitrates through the disproportionation reaction, which is accompanied by the evolution of NO and results in the formation of nitrates. This is referred to as the *nitrate route*.

The role of the Pt-Ba interaction in the mechanism of adsorption of NO_x species has been also studied by means of a literature kinetic model,[38] used to simulate the results collected over, both, the physical mixture and the ternary sample.

As already reported in the literature by several authors, the mechanism of adsorption is considered the sum of the two functionalities present in the catalyst, associated with Pt and Ba sites. So, the model describes the storage of NO_x over Pt-BaO/Al_2O_3, considering NO oxidation to NO_2 on Pt/Al_2O_3 and NO_2 storage on Ba/Al_2O_3. In particular, the model consists of 10 elementary reversible steps: adsorption of oxygen, adsorption of NO, adsorption of NO_2 and oxidation of NO to NO_2 at the Pt sites, adsorption of NO_2 onto the BaO site, release of NO into the gas phase and oxidation of BaO to BaO_2, formation of $BaO-NO_3$ and of $Ba(NO_3)_2$, decomposition of BaO_2 to BaO and oxygen, and the reversible spillover step of NO_2 between Pt sites and BaO sites. Essentially the model assumes that the adsorption of NO_x proceeds through the *nitrate route* and does not consider the *nitrite route*.

Olsson et al.[38] estimated part of the rate parameters in their model from theoretical considerations, part were taken from the literature and calculated from thermodynamic constraints, and part were estimated by fitting a set of experimental data.

At first the model has been used to simulate the experimental results of NO adsorption in the presence of oxygen collected over the physical mixture

of Pt/γ-Al_2O_3 and Ba/γ-Al_2O_3, having the same Pt and Ba loading of the Pt-Ba(16)/γ-Al_2O_3 sample (Figure 12A, dotted lines). The same parameters estimated by *Olsson* et al. have been used for the simulation, but Pt and Ba dispersions were fitted to the experimental data.[39]

As shown in the Figure 12A (solid lines), the model reasonably simulates both, the oxidation of NO to NO_2 and the dead time for the breakthrough of NO_x, as indeed expected. It can be assumed, that the mechanism of NO_x adsorption operating on the physical mixture, e.g. in the absence of any interaction between Pt and Ba atoms, is the *nitrate route* (see Figure 11): NO is oxidized to NO_2 on Pt sites and then adsorbed on Ba (and Al sites) through the disproportion reaction. The reoxidation of NO (which is released from the disproportion reaction) to NO_2 results in a significant NO_x breakthrough also in this case. Hence, the data on the physical mixture confirms the feasibility of the NO_x storage mechanism proposed in literature implying the oxidation of NO to NO_2, followed by NO_2 adsorption on the catalytic surface to form nitrates. In this case, no direct interaction is necessary to have a good and efficient adsorption.
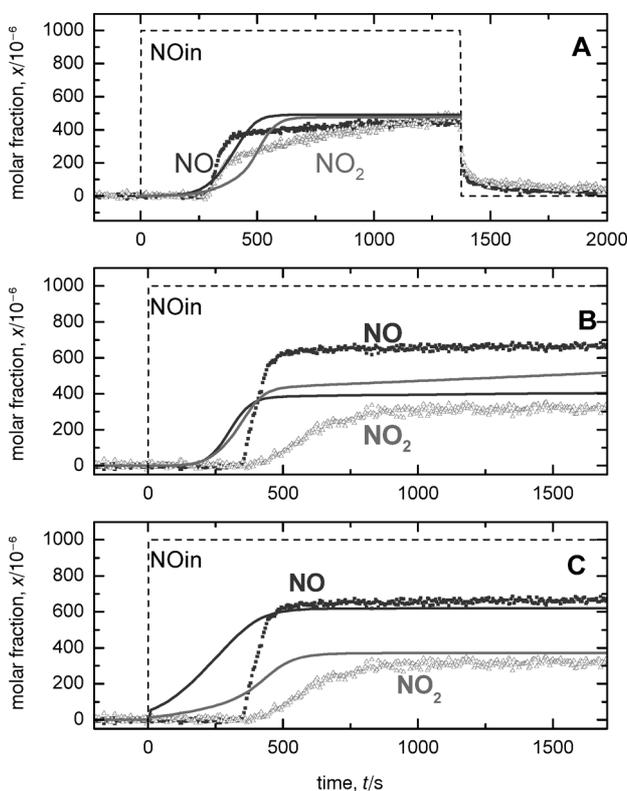
F i g . 1 2 – *NO and NO_2 molar fraction vs time for NO/O_2 TRM experiment at 350 °C over A) the physical mixture Pt/Al_2O_3 + Ba/Al_2O_3: experimental data (symbols) and modelling (solid lines); B) over the ternary Pt-Ba(16)/Al_2O_3 catalyst: experimental data (symbols) and modelling (solid lines); C) over the ternary Pt-Ba(16)/Al_2O_3 catalyst experimental data and modelling from new simulation.*

In the case of the Pt-Ba/alumina the dead time in the NO$_x$ breakthrough upon a step change of NO in the presence of oxygen is reasonably well predicted by the model (see Figure 12B), but the oxidation of NO to NO$_2$ is markedly overestimated.

The Pt dispersion in the model must be lowered to describe properly the oxidation of NO to NO$_2$ but in this case the time delay in the breakthrough of NO$_x$ is no longer predicted (Figure 12C). Therefore, the literature model is not able to describe at the same time the oxidation of NO to NO$_2$ and the storage of NO$_2$ over the ternary Pt-Ba/γ-Al$_2$O$_3$ system.

As a matter of fact these two catalyst properties are strictly interrelated within the *nitrate route*. Accordingly, the nitrate route cannot account for the storage of NO$_x$ under conditions of industrial interest (presence of NO in excess of oxygen).

From data presented so far, it seems evident that the *nitrite route* requires not only the co-presence of Pt and Ba components, but also a cooperative effect between Pt and Ba. This cooperation implies a sort of interaction between these two catalyst components.

The effect of the Pt-Ba interaction, that represents a key feature of the *nitrite route*, has been investigated by preparing Pt-Ba/alumina catalysts with different Ba loading.[40]

The existence of Pt-Ba proximity over the ternary Pt-Ba(16)/γ-Al$_2$O$_3$ sample was investigated by CO chemisorption.[32] The intensity of the FTIR band of CO linearly adsorbed on Pt (observed at 2070 cm^{-1}) decreases on increasing the Ba loading and is progressively shifted towards higher frequencies due to the increasing basic character of the catalysts. This indicates that the interaction between Pt and Ba increases on increasing the Ba loading.

The effect of the Ba loading on the mechanism of NO$_x$ adsorption has been studied by performing TRM experiments with r_{NO/O_2} mixtures at 350 °C over the various samples.

Upon a step change of NO at the inlet in the presence of oxygen the dead time in the breakthrough of NO$_x$ (i.e. the NO$_x$ storage capacity) increases with the Ba mass fraction and is maximum at $w = 23$ % Ba, as shown in Figure 13. Besides the $r_{NO_2/NO}$ molar ratio (which can be related to the oxidizing capacity of the system) is almost constant up
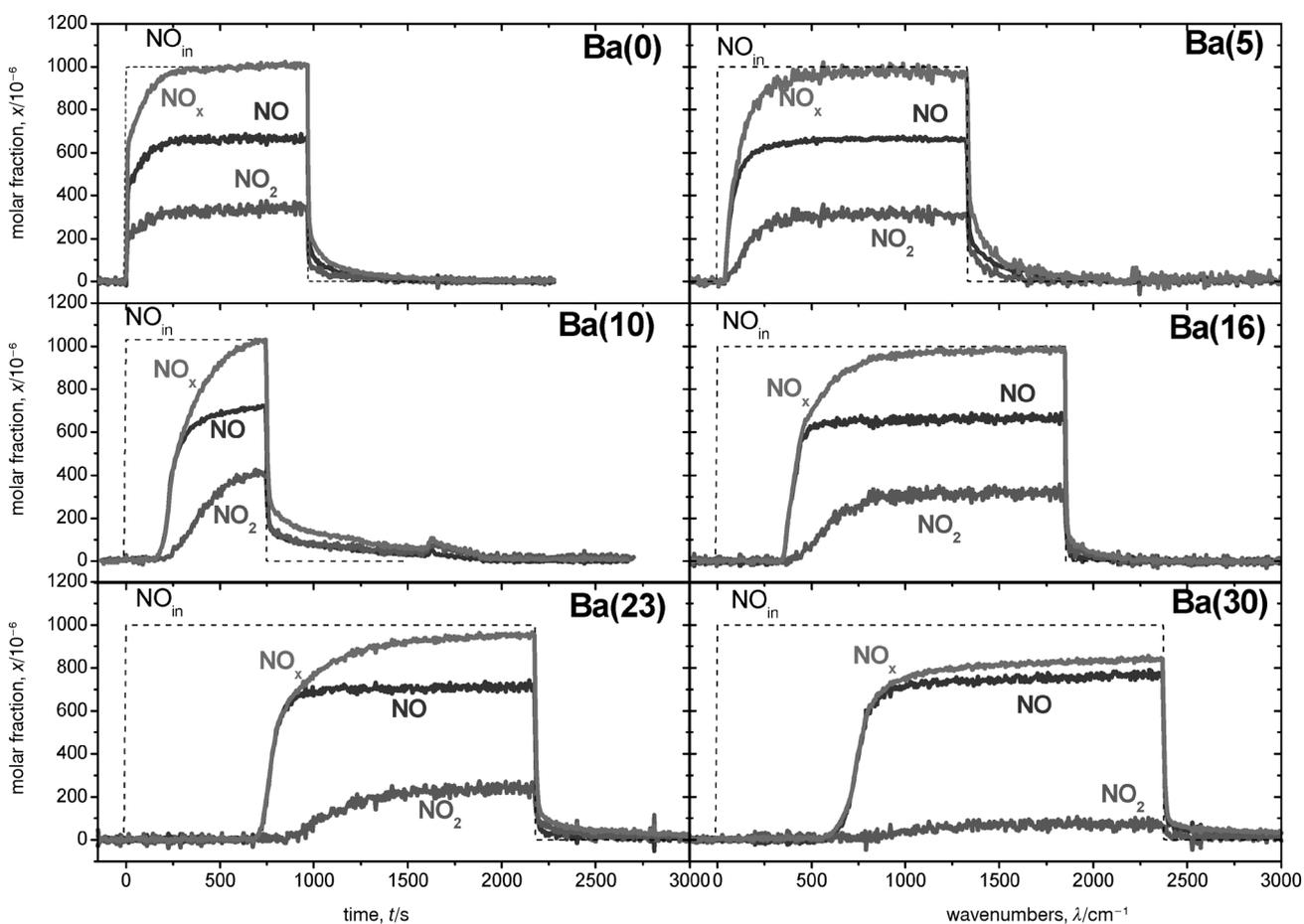
F i g . 1 3– *NO, NO$_2$ outlet molar fraction and NO inlet fraction vs time upon NO addition on the Pt-Ba(x)/γ-Al$_2$O$_3$ catalysts at 350°C: Ba(0); Ba(5); Ba(10); Ba(16); Ba(23) and Ba(30) catalysts*

to 16 % Ba, but it is markedly lower at very high Ba loading (i.e. w = 30 % Ba).

Considering the fraction of Ba that participates in the storage process ("active" Ba), i.e. the molar ratio (%) of Ba involved in the storage with respect to the total amount of Ba present in the catalyst sample, it appears that the fraction of Ba involved up to NO$_x$ breakthrough is low (about 4 %) for Pt-Ba(5) sample, and then increases linearly with the catalyst Ba content, and up to the maximum value of about 25 % for the Pt-Ba(23) sample, which accordingly exhibits the best exploitation of the Ba component.

On the basis of the evidence collected for the Pt-Ba interaction, the results can be explained considering that at low Ba loading the interaction between Pt and Ba is low and the behaviour results from the superposition of that of the two single components: Pt oxidizes NO to NO$_2$ and NO$_2$ undergoes disproportionation over Ba (and possibly alumina). In this case the storage of NO$_x$ proceeds primarily through the nitrate route (see Figure 11) but notice that the NO$_x$ breakthrough occurs with a short dead time.

At high Ba content the interaction between the two components is favoured by their proximity. In this case the storage of NO$_x$ occurs primarily through the nitrite route: NO is oxidised over Pt and is adsorbed at a neighbouring Ba site in the form of a nitrite species that is then oxidized to a nitrate species. In this case the storage of NO$_x$ is characterised by a significant dead time in the NO$_x$ breakthrough.

Conclusions

The bulk of the information gained by the current transient experiments, coupled with the FTIR spectra, helped in clarifying reaction pathway for the storage of NO$_x$ species over Pt-Ba/Al$_2$O$_3$ catalyst from NO/O$_2$. The most important features include:

i) On Pt-Ba/Al$_2$O$_3$ catalysts the storage of NO$_x$ occurs through both a *nitrite* and a *nitrate* route.

ii) The *nitrite* route implies a stepwise oxidation of NO at Pt followed by adsorption at a neighbouring Ba site to form a nitrite ad-species that is then oxidised to a nitrate species.

iii) The *nitrate* pathway implies the oxidation of NO to NO$_2$ at Pt followed by the adsorption in the form of nitrates through the disproportionation reaction of NO$_2$.

iv) On increasing the Ba loading, the *nitrite* route is more favoured than the *nitrate* route due to the higher number of Pt-Ba couples (Pt atoms in close proximity to Ba atoms).

v) The presence of Pt-Ba couples enhances the exploitation of the Ba component in the storage of NO$_x$.

vi) The *nitrite route* is most effective under conditions of industrial interest.

Notation

V	– superficial velocity, m^3 m^{-2} h^{-1}, m h^{-1}
c_i	– gas-phase concentration of species i, mol m^{-3}
$c_{w,i}$	– concentration of species i at gas-solid interface, mol m^{-3}
$D_{eff,i}$	– effective intraporous diffusivity of species i, m^2/s
d_h	– hydraulic diameter of the monolith channels, m
E_a	– activation energy for NH$_3$ adsorption, kJ mol^{-1}
E_d	– activation energy for NH$_3$ desorption, kJ mol^{-1}
E_d°	– activation energy for NH$_3$ desorption at zero-coverage, kJ mol^{-1}
E_{NO}	– activation energy for the DeNO$_x$ reaction, kJ mol^{-1}
h	– gas-solid heat transfer coefficient, J cm^{-2} s^{-1} K^{-1}
k_a°	– pre-exponential factor for NH$_3$ adsorption rate, m^3 mol^{-1} s^{-1}
k_c	– effective rate coefficient of the surface chemical reaction, m^3 mol^{-1} s^{-1}
k_d°	– pre-exponential constant for NH$_3$ desorption rate, s^{-1}
k_g	– the inter-phase gas-solid mass transfer coefficient, m^3 mol^{-1} s^{-1}
k_{mt}	– gas-solid mass transfer coefficient, m^3 mol^{-3} s^{-1}
K_{NH_3}	– quantity for NH$_3$ inhibition, m^3 mol^{-1}
k_{NO}	– kinetic coefficient for the DeNO$_x$ reaction rate, m^3 mol^{-1} s^{-1}
k_{ox}	– rate coefficient for ammonia oxidation, s^{-1}
k_{SCR}	– intrinsic kinetic coefficient of the SCR reaction, –
L	– monolith length, m
n	– amount of substance, mol
Nu_T	– Nusselt number, –
p	– partial pressure, bar
p_{O_2}	– oxygen partial pressure, bar
r_a	– rate of NH$_3$ adsorption, s
r_d	– rate of desorption, s
$r_{eff,i}$	– effective surface rate of formation of species j, mol m^{-2} s^{-1}
r_i	– intrinsic volumetric rate of formation of species i, mol m^{-3} s^{-1}
r_{NO}	– rate of NO consumption, s^{-1}
r_{ox}	– rate of ammonia oxidation, s^{-1}
r_{NH_3/NO_x}	– molar ratio,
Sh	– Sherwood number
δ_w	– half-thickness of monolith wall, m
T	– temperature, K

t – time, s

T_g – gas temperature, K

T_s – catalyst temperature, K

v – gas linear velocity, m s^{-1}

χ – molar fraction, 10^{-6}

x – dimensionless intraporous coordinate, –

z – reactor axial coordinate, m

z – dimensionless reactor axial coordinate, –

$\Delta H_{f,i}$ – enthalpy of formation of species i, J mol^{-1}

w – mass fraction, %, 10^{-2}

Greek letters

γ – parameter for the surface coverage dependence

ρ – volume fraction, %, 10^{-2}

η – catalyst internal efficiency

θ_i – surface coverage of species i

χ_{NO_x} – the fractional conversion of NO$_x$

$\theta_{NH_3}^*$ – parameter for the NH$_3$ surface coverage dependence

ρ_g – gas density, kg m^3

ρ_s – catalyst density, kg m^{-3}

C_{NH_3} – catalyst NH$_3$ adsorption capacity, mol m^{-3}

ζ – mass ratio

Subscripts and superscripts

b   – bulk gas conditions

eff   – effective rate

f   – free sites

m   – cup-mixing cross-sectional average

w   – conditions at the monolith wall

°   – conditions at reactor inlet

*   – dimensionless quantity

∞ – asymptotic value for $z^* \to \infty$

References

1. *Forzatti, P., Lietti, L., Tronconi, E.,* "Nitrogen oxides removal – Industrial" in Encyclopedia of Catalysis, 1st Ed.; I.T Horvath, Ed.; J. Wiley and Sons: New York, 2002.

2. *Epling, W. S., Campbell, L. E., Yezerets, A., Currier N. W., Park II J. E.,* Catal.Reviews, **46(2)** (2004) 163.

3. *Forzatti, P.,* Catal. Today, **62** (2000) 51

4. *Boer, F. P., Hegedus, L. L.,. Gouker, T. R, Zak, K. P.,* ChemTech, **312** (1990).

5. *M. Takagi, T. Kowai, M. Soma, T. Onishi, T., K. Tamaru,* J. Catal., **50** (1977) 441.

6. *Inomata, M., Miyamoto, A., Muratami, Y.,* J. Catal., **62** (1980) 140.

7. *Ramis, G. Busca, G. Bregani, F., Forzatti, P.* Appl. Catal., **64** (1990) 259

8. *Topsøe, N. Y., Topsøe, H., Dumesic, J. H.,* J. Catal., **151** (1995) 226.

9. *Topsøe, N. Y., Topsøe, H., Dumesic, J. H.,* J. Catal., **151** (1995) 241.

10. *Svachula, J., Ferlazzo, N., Forzatti, P., Tronconi E., Bregani, F.,* Ind. Eng. Chem. Res., **32 (6)** (1993) 1053.

11. *Beeckman, J. W., Hegedus, L. L.,* Ind. Eng. Chem. Res., **30(5)** (1991) 969.

12. *Tronconi, E., Forzatti, P., Gomez Martin, J. P., Malloggi, S.,* Chem. Eng. Sci., **47** (1992) 2401.

13. *Tronconi, E., Forzatti, P.,* AlChE J., **38** (1992) 201.

14. *Beretta, A., Orsenigo, C., Ferlazzo, N., Tronconi, E., Forzatti, P.,* Ind. Eng. Chem. Res., **37** (1998) 2623.

15. *Lietti, L., Nova, I., Camurri, S., Tronconi, E., Forzatti, P.,* AIChE J., **43(10)** (1997) 2559.

16. *Mears, D. E.* Ind. Eng. Chem. Process Des. Develop, **10(4)**, (1971) 541.

17. *Finlayson, B.,* in "Nonlinear Analysis in Chemical Engineering", McGraw Hill Eds. New York, 1980.

18. *Hindmarsh, A. C., i*n "Odepack: a systematized collection of ODE solvers", in Scientific Computing (R.S. Stepleman et al., Ed.s); North Holland, Amsterdam, 1983.

19. *Ramis, G., Busca, G,. Forzatti, P., Cristiani, C., Lietti L., and Bregani, F.,* Langmuir. **8**, (1992) 1744.

20. *Tronconi, E., Nova, I., Ciardelli, C., Chatterjee, D., Bandl-Konrad, B., Burkhardt, T.,* "Modelling of an SCR catalytic converter for Diesel exhaust after treatment: dynamic effects at low temperature", Catal. Today, *in press*

21. *Nova, I., Lietti, L., Tronconi, E., Forzatti, P.,* Catal. Today, **60** (2000) 73.

22. *Nova, I., Lietti, L., Tronconi, E., Forzatti, P.,* Chem. Eng. Sci., **56** (2001) 1229

23. *Chatterjee, D., Burkhardt, T., Bandl-Konrad, B,. Braun, T., Tronconi, E., Nova, I., Ciardelli, C.,* SAE paper 2005-01-965 (2005).

24. *Mahzoul, H., Brilhac, J. F., Gilot, P.,* Appl. Catal. B, **20** (1999) 47.

25. *Cant, N. W., Patterson, M. J.,* Catal. Today, **73** (2002) 271.

26. *Fridell, E., Skoglundh, M., Westerberg, B., Johansson, S., Smedler, G.,* J. Catal., **183** (1999) 196.

27. *Fridell, E., Persson, H., Westerberg, B., Olsson, L., Skoglundh, M.,* Catal. Lett., **66** (2000) 71.

28. *Westerberg, B., Fridell, E.,* J. Mol. Catal. A: Chem., **165** (2001) 249.

29. *Anderson, J. A., Bachiller-Baeza, B., Fernández-García, M.,* Phys. Chem. Chem. Phys., **5** (2003) 4418.

30. *Hess, C., Lunsford, J. H.,* J. Phys. Chem. B, **106** (2002) 6358.

31. *Lietti, L., Forzatti, P., Nova, I., Tronconi, E.,* J. Catal., **204** (2001) 175.

32. *Prinetto, F., Ghiotti, G., Nova, I., Lietti, L., Tronconi, E., Forzatti, P.,* J. Phys. Chem.B. **105** (2001) 12732.

33. *Nova, I., Castoldi, L., Lietti, L., Tronconi, E., Forzatti, P.,* Catal. Today, **75** (2002) 431.

34. *Castoldi, L., Nova, I., Lietti, L., Tronconi, E., Forzatti, P.,* Chem. Eng. Trans., **3** (2003) 117.

35. *Nova, I., Castoldi, L., Prinetto, F., Dal Santo, V., Lietti, L., Tronconi, E., Forzatti, P., Ghiotti, G., Psaro, R., Recchia, S.,* Top. Catal., **30/31** (2004) 181.

36. *Prinetto, F., Ghiotti, G., Nova, I., Castoldi, L., Lietti, L., Forzatti, P.,* Phys. Chem. Chem. Phys., **5** (2003) 4428.

37. *Nova, I., Castoldi, L., Lietti, L., Tronconi, E., Forzatti, P., Prinetto, F., Ghiotti, G.,* J. Catal., **222** (2004) 377.

38. *Olsson, L., Persson, H., Fridell, E., Skoglundh, M., Andresson, B.,* J. Phys. Chem. B, **105** (2001) 6895

39. *Scotti, A., Nova, I., Tronconi, E., Castoldi, L., Lietti, L., Forzatti, P.,* Ind.Eng.Chem.Res., **43 (**2004) 4522.

40. *Castoldi, L., Nova, I., Lietti, L., Forzatti, P.,* Catal. Today, **96** (2004) 43